Supplementary Information (SI) for ChemComm.
This journal is © The Royal Society of Chemistry 2026

Supporting information

Stability and Degradation Mechanisms of Silver-Nickel Nanoparticle Catalysts for Electrochemical CO_2 Reduction

Yan Wang[a], Rui Xue[a], Nan Wang[b], Lu Ma[c], Yiming Chen[a], Qingquan Yang[a], Xiaohui Yan[a], Zulipiya Shadike[a], Shuiyun Shen*[a], and Junliang Zhang*[a]*

a. Institute of Fuel Cells, School of Mechanical Engineering, Shanghai Jiao Tong University, Shanghai 200240, China.

b. Department of Materials Science, Department of Chemistry, Shanghai Key Laboratory of Molecular Catalysis and Innovative Materials, Fudan University, Shanghai 200433, China.

c. National Synchrotron Light Source II, Brookhaven National Laboratory, Upton, NY 11973, USA.

* E-mail: zshadike@sjtu.edu.cn; shuiyun_shen@sjtu.edu.cn; junliang.zhang@sjtu.edu.cn

Experimental Methods

Materials

The following chemicals were used without further purification: reverse osmosis (RO) water, Silver nitrate ($AgNO_3$, AR), Nickel sulfate hexahydrate ($NiSO_4 \cdot 6H_2O$, AR), Polyvinylpyrrolidone (PVP, average mol wt 10000), Sodium borohydride ($NaBH_4$, AR), Acetone (C_3H_6O, AR), Isopropanol (C_3H_8O, AR), Potassium bicarbonate ($KHCO_3$, 99.5%), Nafion solution (5wt%), Carbon paper.

Preparation of electrode

Synthesis of Pure Ag catalyst. The pure Ag catalyst was synthesized via a liquid-phase reduction method. Briefly, 339.72 mg of $AgNO_3$ and 1 g of PVP were dissolved in 100 mL of RO water (the concentration of $AgNO_3$ was 20 mM). Subsequently, 10 mL of a 789 mM $NaBH_4$ solution was added dropwise under vigorous stirring. The resulting brown–black Ag hydrosol was allowed to stand for 30 min to decompose residual $NaBH_4$. To isolate the Ag nanoparticles, 50 mL of acetone was then added to the aged dispersion to remove PVP. After standing for another 24 h, the black precipitate was collected and washed three times with RO water to obtain Ag nanoparticles.

Synthesis of Ag-Ni catalysts. The Ag-Ni catalysts were synthesized following the same procedure as that for the pure Ag catalyst, except that a part of the $AgNO_3$ precursor was replaced with $NiSO_4$ while keeping the total concentration of Ag^+ and Ni^{2+} ions in solution at 20 mM. A series of catalysts with different Ni molar fractions was thereby obtained, denoted as Ag-2%Ni, Ag-5%Ni, and Ag-10%Ni (e.g., for Ag-10%Ni, the concentration of Ni^{2+} in the precursor solution was 2 mM). Finally, the pure Ni catalyst was prepared by substituting all Ag^+ with Ni^{2+}.

Preparation of working electrode. The washed nanoparticle catalyst was dispersed in 60 mL mixture of RO water and isopropanol (volume ratio of 2:1). Subsequently, 0.8 mL of Nafion solution was added, and the resulting suspension was sonicated until homogeneous. An appropriate amount of the resulting ink was spray-coated onto carbon paper preheated to 95 °C, with the catalyst loading controlled at 0.25 mg cm^{-2}. After thorough drying, the coated carbon paper was annealed at 300 °C for 2 h under a nitrogen atmosphere to obtain the working electrode.

Fig. S1 Synthesis of catalyst and preparation working electrode.

Characterization

Electrochemical measurement. The electrochemical performance was analysed in a flow cell consisting of a gas chamber, cathode and anode chambers. The working electrode with a geometric surface area of $1cm^2$ was sandwiched between the gas chamber and the cathode chamber. The PiperION Self-Supporting anion exchange membrane was used to separate the cathode and anode chambers. A platinum mesh was used as the counter electrode in the anode chamber. Ag/AgCl was used as reference electrode, and calibrated against a reversible hydrogen electrode (RHE) before the test. Ohmic drop compensation was performed based on EIS measurements. The electrode potentials were rescaled to the RHE reference by the following equation:

$$E(vs.\,RHE) = E(vs.\,Ag/AgCl) + 0.1976\,V + 0.0591 \cdot pH - iR_u$$

Autolab PGSTAT302N electrochemical workstation was used for the electrochemical measurement. The electrochemical performance test included linear sweep voltammetry (LSV), product selectivity test and stability test. See the SI for the specific parameter settings of each test. During the experiment, pure CO_2 with flow rate is controlled at 20 SCCM was introduced into the gas chamber. A 0.5 M $KHCO_3$ solution (0.1 M for stability tests) was circulated through the peristaltic pump in the cathode and anode chambers,

respectively. After passing through the drying tube, the gas product was introduced into the gas chromatograph GC-2014 for component analysis. The concentration and FE of each product were calculated from the integrated peak areas.

$$FE_i = \frac{z_i F P C_i F_{gas}}{jART} \times 100\%$$

ECSA measurement. Cyclic voltammetry (CV) was employed to determine the double-layer capacitance of the working electrode, which was further used for a qualitative comparison of the electrochemical active surface area (ECSA) among different catalysts. A series of cyclic voltammetry curves was recorded within the same potential window (-0.15 to 0.05 V vs. Ag/AgCl) at scan rates ranging from 5 to 15 $mV \cdot s^{-1}$. Each condition was measured 8 times, and the averaged response curve was used for analysis. At a given potential, the anodic and cathodic current densities, denoted as j_a and j_c, respectively, were extracted from the forward and reverse scans, and the capacitive current density was calculated as

$\Delta j = (j_a - j_c) / 2$

A linear fit of Δj versus the scan rate was then performed, and the slope was taken as the double-layer capacitance (C_{dl}). The ECSA can be expressed as

$ECSA = C_{dl} / C_s$

where C_s is affected by factors such as the electrolyte composition, potential window, and other test conditions. In this study, all catalysts were measured under identical experimental conditions; therefore, C_s can be regarded as a constant. On this basis, the ECSA of different catalysts can be qualitatively compared by comparing their C_{dl}.

Characterization of materials structure. Inductively coupled plasma–atomic emission spectroscopy (ICP-AES) was obtained using Avio 500. Powder X-ray diffraction (XRD) measurements were conducted on a Rigaku Mini Flex 600 X-ray diffractometer with Cu Kα1 radiation of 1.54 Å (V = 40 kV, I = 15 mA). Transmission electron microscope (TEM) images were obtained with a Field Emission Transmission Electron Microscope (Talos F200X G2). Catalysts for TEM characterization were embedded and sectioned prior to analysis. Scanning electron microscopy (SEM) images were obtained using a field emission scanning electron microscope (Gemini 360). X-ray photoelectron spectroscopies (XPS) measurements were performed using an ESCALAB QXi energy spectrometer. Hard XAS characterizations were conducted at the 7-BM (QAS) beamline of National Synchrotron Light Source II (NSLS-II) at Brookhaven National Laboratory. The XANES and EXAFS data were processed and normalized by utilizing Athena software packages.[23]

Supporting Tables

Table S1 Parameter settings of electrochemical performance tests.

LSV:

Parameter	Value
Potential Range (V vs. RHE)	-1.6~0
Scan rate (V/s)	0.05
Scan step (V)	0.00244

Product Selectivity Test:

Parameter	Value
Potential Range (V vs. RHE)	-1.6~-0.8
Scan step (V)	0.1
Duration (s)	600

Stability Test:

Parameter	Value
Potential (V vs. RHE)	-1.4
Duration (h)	30

Table S2 The performance of Ag based catalysts in recent years. (*: the catalyst reported in this work. The values in parentheses refer to the current density at the corresponding potential.)

Catalyst	Optimal FE_{CO} (%)	Potential vs. RHE (V)	Low limit (V)	Up limit (V)	j_{CO} ($mA \cdot cm^{-2}$)	Cell type	Electrolyte
2D Ag-SS[1]	96.3	-0.6	-0.9	-0.3	4	H cell	0.1 M KOH
Ag-900D NNAs[2]	91.4	-1	-1.6	-0.8	12	H cell	0.5 M $KHCO_3$
2 nm-Ag NCs[3]	93.8	-0.756	-1.1	-0.5	2.36	Home made	0.1 M $KHCO_3$
L25-Ag-NCs[4]	99	-0.856	-1.1	-0.5	1.6	Custom built	0.1 M $KHCO_3$
P-Ag[5]	94	-0.735	-1.14	-0.64	1.8	flow cell	KOH
re-AgS4[6]	98.13	-1.1	-1.2	-0.75	32.7	H cell	0.1 M $KHCO_3$
Ag/GDY/CC[7]	92.1	-1.3	-1.4	-1	25.74	H cell	0.1 M $KHCO_3$
Ag/d-HOPG[8]	100	-1.3	-1.3	-0.9	/	H cell	0.1 M $KHCO_3$
CV-activated Ag[9]	96.6	-0.7	-1.1	-0.7	7.4	H cell	0.5 M $KHCO_3$
Ag1-AgAC@NCNT[10]	99	-0.3	-0.9	-0.3	29.3	flow cell	1 M KOH
Ag2-G[11]	93.4	-0.7	-1	-0.3	11	H cell	0.5 M $KHCO_3$
Ag_{15}(C C-tBu)$_{12}^{+12}$	95	-0.6	-1.1	-0.5	2	H cell	0.5 M $KHCO_3$
np-AgCe-2[13]	98	-0.8	-2	-0.8	50	flow cell	1 M KOH
$Au_{50}Ag_{50}$-1 AG[14]	97.8	-0.7	-0.9	-0.5	5.29	H cell	0.1 M $KHCO_3$
Ag/[Co_3Ni(bpy)$_3$]$^{2+}$[15]	98	-1	-0.5	-1.3	19	H cell	0.5 M KHCO3
$Ag_{96}Cu_4$[16]	98.7	-1	-1.2	-0.6	6	H cell	0.1 M $KHCO_3$
Cr_2O_3@Ag[17]	99.6	-0.8	-1.3	-0.5	20	H cell	0.5 M $KHCO_3$
Ag–Ni/CB[18]	99.3	-0.8	-1.2	-0.7	7	H cell	0.1 M $KHCO_3$
NiAD/AgNPs @CN[19]	91.77	-0.88	-1.1	-0.6	79.7	flow cell	1 M KOH
Ni_3Ag_2(S-cy)$_8$[20]	100	-0.8	-2	-0.5	130	flow cell	1 M KOH
Ni-Ag/PC[21]	99.2	-0.8	-1.3	-0.7	13	H cell	0.1 M $KHCO_3$
Ag-5%Ni*	97.8	-1.5(120)	-1.9(180)	-0.9(40)	120	flow cell	0.5 M $KHCO_3$

Table S3 The stability performance of Ag based catalysts in recent years. (*: the catalyst reported in this work.)

Catalyst	Time (h)	Current density ($mA \cdot cm^{-2}$)	FE_{CO} (%)
2D Ag-SS[1]	100	3.5	95
Ag-900D NNAs[2]	12	11	90
2 nm-Ag NCs[3]	45	1.2	83
L25-Ag-NCs[4]	18	1.1	90
P-Ag[5]	10	3	83
re-AgS4[6]	50	30	87
Ag1-AgAC@NCNT[10]	10	100	100
Ag2-G[11]	36	12	86.8
$Ag_{15}(C\ C\text{-}tBu)_{12}^{+}$[12]	9	7.5	85
np-AgCe-2[13]	16.7	50	100
$Au_{50}Ag_{50}$-1 AG[14]	18	5.2	89
$Ag/[Co_3Ni(bpy)_3]^{2+}$[15]	9	1.5	54.3
Ag-Co[22]	12	23.3	90
$Ag_{96}Cu_4$[16]	10	6	90.2
Cr_2O_3@Ag[17]	25	18.2	97.6
Ag–Ni/CB[18]	11.5	6.4	93.7
NiAD/AgNPs@CN[19]	11	5.1	95.2
Ag-5%Ni*	50	25	95

Table S4 The Ni content in the Ag–Ni catalysts.

Catalyst	Ni (wt%)	Ni (mol%)	Nominal value (mol%)
Ag-2%Ni	1.057	1.893	2
Ag-5%Ni	2.537	4.491	5
Ag-10%Ni	5.027	8.722	10

Table S 5 ANOVA of the particle size in Fig. S 13.

Catalyst		Mean	SE	F	p
Pure Ag	Before test	0.36572 μm	0.128	72.30761	<0.0001
	After test	0.70391 μm	0.24074		
Ag-5%Ni	Before test	45.73308 nm	11.0454	1.31457	0.25389
	After test	47.86605 nm	9.2548		

Supporting Figures

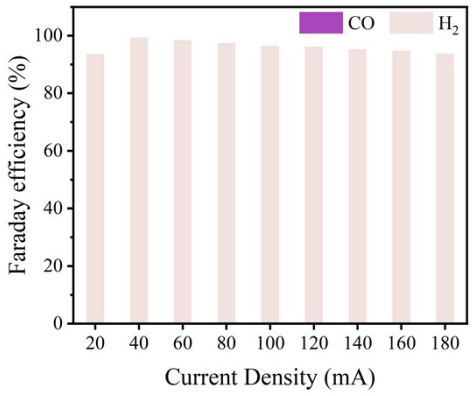

Fig. S2 Product selectivity results of pure Ni catalyst.

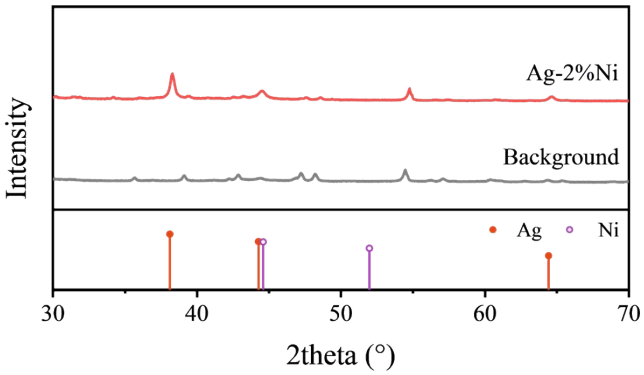

Fig. S3 XRD patterns of Ag-2%Ni catalyst.

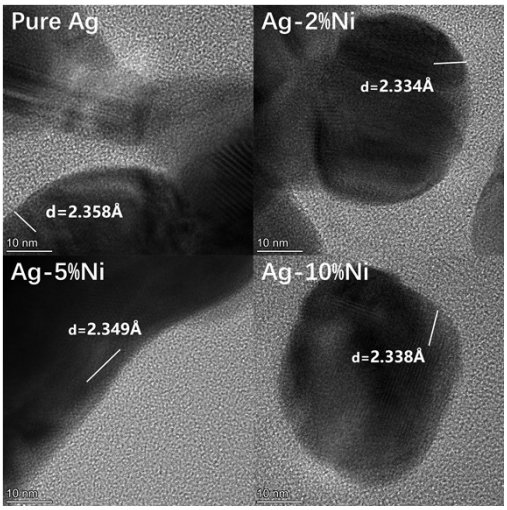

Fig. S4 Transmission electron microscopy (TEM) images and lattice spacings of pure Ag and Ag-Ni catalysts.

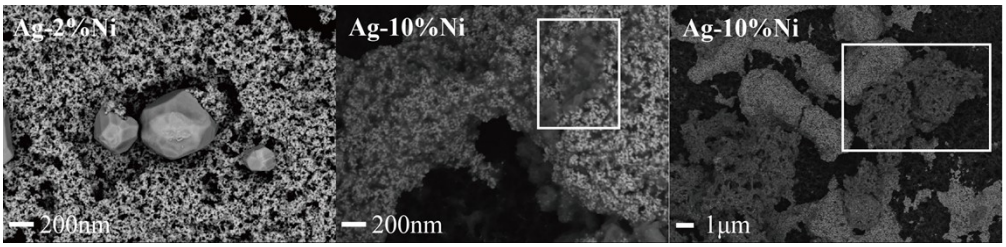

Fig. S5 SEM backscattered electron (BSE) images of the Ag-2%Ni (left 20k x) and Ag-10%Ni catalysts (middle 20k x; right 3k x).

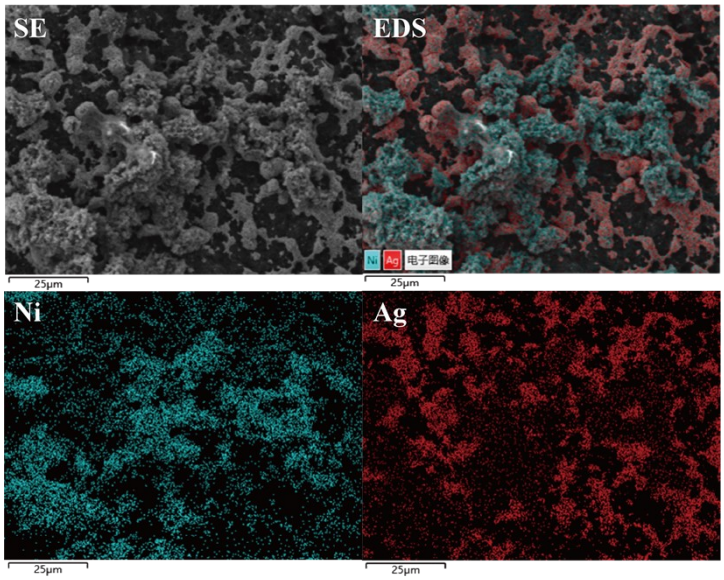

Fig. S6 EDS elemental mapping of the Ag-10%Ni catalyst.

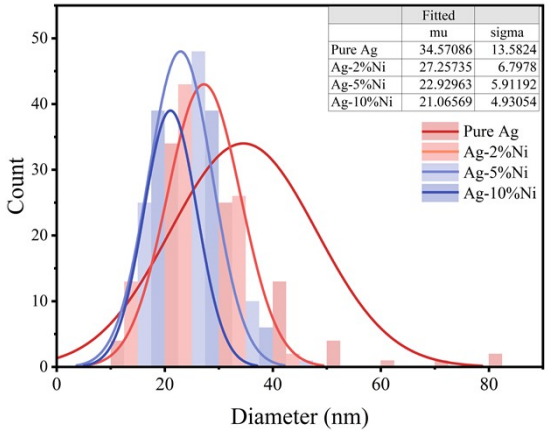

Fig. S7 Particle size distributions of pure Ag and Ag-Ni catalysts (histograms of particle diameters with fitted distribution curves).

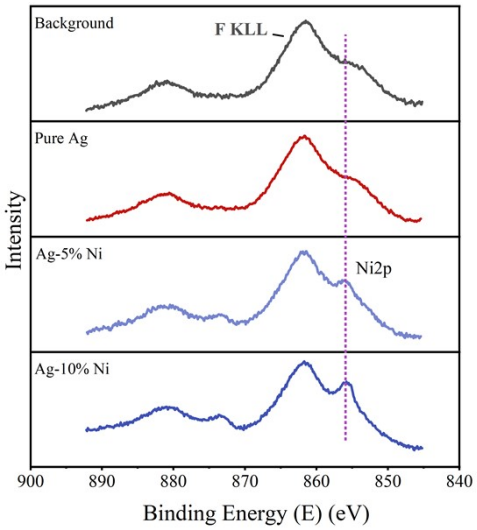

Fig. S8 X-Ray spectra Spectrometer of Ni in pure Ag, Ag-5%Ni and Ag-10%Ni. The positions of the Ni2p peaks are marked by purple dashed lines. The other miscellaneous peaks arise from the Auger peaks of F present in the carbon paper background.

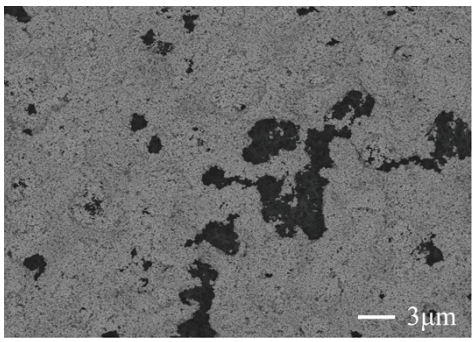

Fig. S9 SEM image of Ag-5%Ni before stability test (3k x).

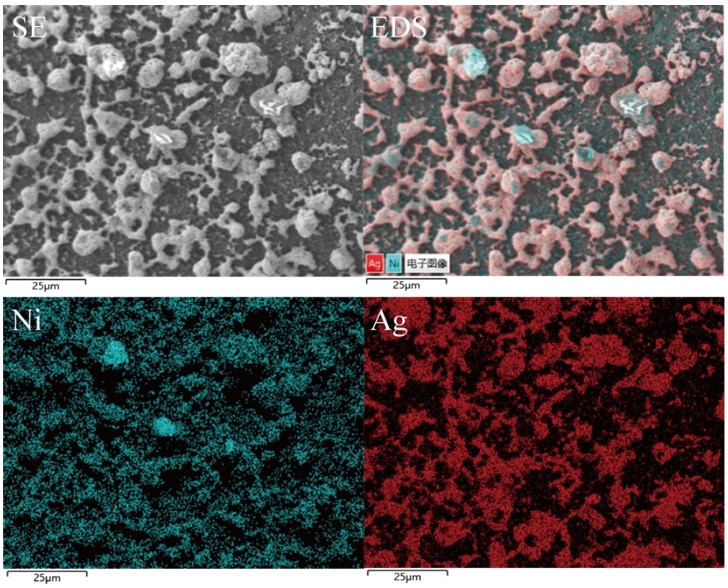

Fig. S10 EDS mapping of Ag-5%Ni after stability(100mA/cm^2).

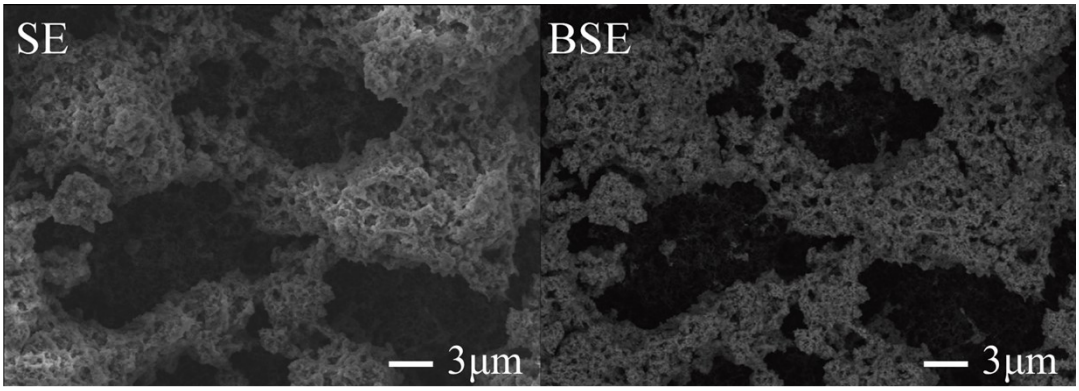

Fig. S11 SEM images of pure Ni catalyst (3k x.).

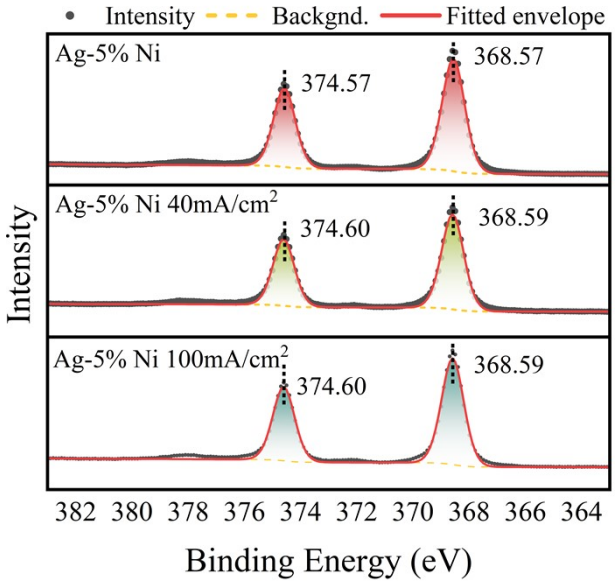

Fig. S12 XPS images of Ag-5%Ni after stability tests.

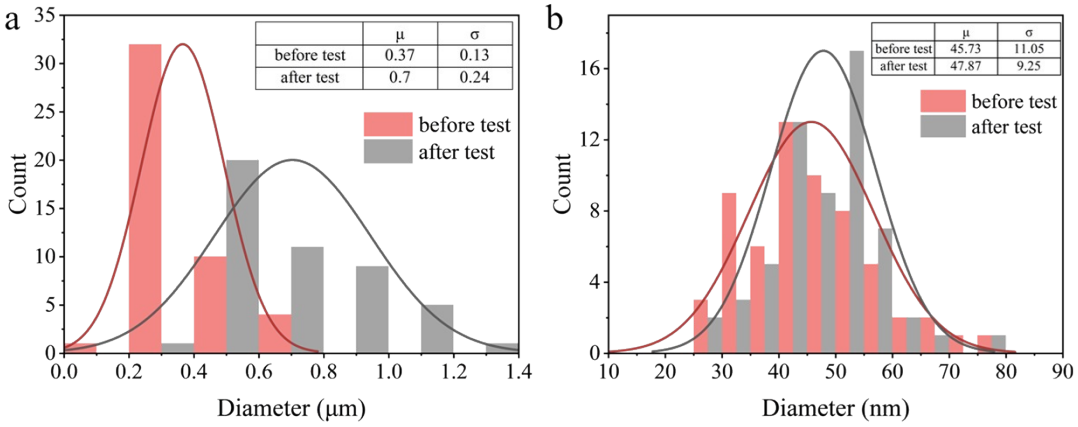

Fig. S 13 Particle size statistics of the pure Ag (a) and Ag-5%Ni (b) before and after the stability test at 100 mA·cm^{-2}.

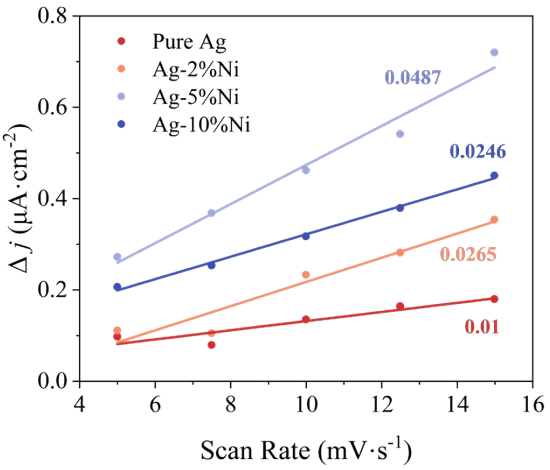

Fig. S 14 Linear fitting results of Δj versus scan rate for ECSA estimation. the numbers in the figure represent the slopes of the corresponding fitted lines.

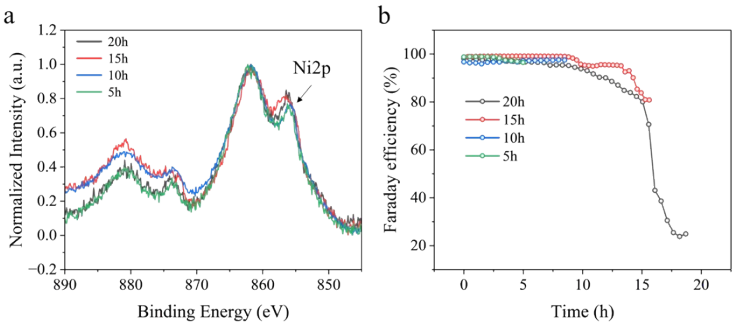

Fig. S 15 (a) XPS Ni2p spectra of Ag-5% Ni after stability test. (b) FE_{CO} of stability test for different duration.

References of SI

1 K. Qi, Y. Zhang, J. Li, C. Charmette, M. Ramonda, X. Cui, Y. Wang, Y. Zhang, H. Wu, W. Wang, X. Zhang and D. Voiry, *ACS Nano*, 2021, **15**, 7682–7693.

2 Q. Chen, K. Liu, Y. Zhou, X. Wang, K. Wu, H. Li, E. Pensa, J. Fu, M. Miyauchi, E. Cortés and M. Liu, *Nano Letters*, 2022, **22**, 6276–6284.

3 H.-C. Mi, C. Yi, M.-R. Gao, M. Yu, S. Liu and J.-L. Luo, *ACS Applied Materials & Interfaces*, 2022, **14**, 43257–43264.

4 S. Liu, C. Sun, J. Xiao and J.-L. Luo, *ACS Catalysis*, 2020, **10**, 3158–3163.

5 S.-Q. Liu, S.-W. Wu, M.-R. Gao, M.-S. Li, X.-Z. Fu and J.-L. Luo, *ACS Sustainable Chemistry & Engineering*, 2019, **7**, 14443–14450.

6 J. Chen, X. Liu, S. Xi, T. Zhang, Z. Liu, J. Chen, L. Shen, S. Kawi and L. Wang, *ACS Nano*, 2022, **16**, 13982–13991.

7 W. Xie, S. Zhang, Y. Ni, G. Shi, J. Li, X. Fu, X. Chen, M. Yuan and M. Wang, *Advanced Energy and Sustainability Research*, 2021, **2**, 2100037.

8 X. Deng, D. Alfonso, T.-D. Nguyen-Phan and D. R. Kauffman, *ACS Catalysis*, 2023, **13**, 15301–15309.

9 Y. Mao, Q. Mao, H. Yang, Q. Liu, X. Dong, Y. Li, S. Zhou and B. Liu, *Angewandte Chemie International Edition*, 2024, **63**, e202410932.

10 Y. Xu, X. Zhang, C. Yang, C. Gong, X. Qin, H. Sun, H. Chen, M. A. Soldatov, K. Zheng, C. Li, T. Gan, J. Li, J. He and Q. Liu, *Advanced Energy Materials*, 2024, **14**, 2400143.

11 Y. Li, C. Chen, R. Cao, Z. Pan, H. He and K. Zhou, *Applied Catalysis B: Environmental*, 2020, **268**, 118747.

12 L. Qin, F. Sun, X. Ma, G. Ma, Y. Tang, L. Wang, Q. Tang, R. Jin and Z. Tang, *Angewandte Chemie International Edition*, 2021, **60**, 26136–26141.

13 Z. Li, X. Zhou, Y. Liu, X. Li, Y. Shen, M. Wen, P. Lei and L. Qian, *ACS Catalysis*, 2025, **15**, 15019–15032.

14 J. Mo, D. Lou, J. Li, X. Tao, Z. Zheng and W. Liu, *Journal of Colloid and Interface Science*, 2025, **697**, 137934.

15 X. Jiang, W. Chu, X. Ren, F. Ma, R. Chen, S. Ning, Y. Zhang, C. Zeng, L. Shi, L. Ren, X. Qi, H. Zhang, H. Ni and J. Ye, *ACS Nano*, 2025, **19**, 17336–17346.

16 M. Li, Y. Hu, G. Dong, T. Wu and D. Geng, *Small*, 2023, **19**, 2207242.

17 H. Q. Fu, J. Liu, N. M. Bedford, Y. Wang, J. W. Sun, Y. Zou, M. Dong, J. Wright, H. Diao, P. Liu, H. G. Yang and H. Zhao, *Advanced Materials*, 2022, **34**, 2202854.

18 H. Wang, Z. Guo, H. Zhang, L. Jia, M. Sun, L. Han, H. Li, Y. Guo and S. Zeng, *Catalysis Science & Technology*, 2025, **15**, 154–164.

19 Z. Zhao, L. Lin, Y. Ni, L. Jin, L. Feng, Y. Wang, Y. Wei, J. Zhang and J. Chen, *Applied Catalysis B: Environment and Energy*, 2024, **349**, 123886.

20 F. Tian, W. Li, W. Guo, G. Li and R. Chen, *Science China Materials*, 2023, **66**, 407–412.

21 Guo Z., Zhu H., Yang G., Wu A., Chen Q., Yan Z., Loon Fow K., Do H., Hirst J. D., Wu T. and Xu M., *Chemical Engineering Journal*, 2023, **476**, 146556.

22 Y. Qin, W. Qian, J. Zhang, X. Chen, M. Chen, X. Qin and C. Zhang, *Electrochimica Acta*, 2025, **514**, 145637.

23 B. Ravel and M. Newville, J Synchrotron Radiat, 2005, **12**, 537–541.